LAWRENCE
LIVERMORE
NATIONAL
LABORATORY

LLNL-JRNL-404415

Mapping of Proteomic Composition on the Surfaces of Bacillus spores by Atomic Force Microscopy-based Immunolabeling

M. Plomp, A. J. Malkin

June 3, 2008

Langmuir

Disclaimer

Mapping of Proteomic Composition on the Surfaces of *Bacillus* spores by Atomic Force Microscopy-based Immunolabeling

Marco Plomp and Alexander J. Malkin[†]

Department of Chemistry, Materials, Earth and Life Sciences, Lawrence Livermore National Laboratory, L-233, Livermore CA 94551, USA;

[†] Corresponding author: Mailing address: Department of Chemistry, Materials, Earth, and Life Sciences, L-233, Lawrence Livermore National Laboratory, 7000 East Avenue, Livermore CA 94551. Phone: (925) 423-7817; FAX: (925) 422-2041. E-mail: **malkin1@llnl.gov**

Abstract

Atomic force microscopy provides a unique capability to image high-resolution architecture and structural dynamics of pathogens (e.g. viruses, bacteria and bacterial spores) at near molecular resolution in native conditions. Further development of atomic force microscopy in order to enable the correlation of pathogen protein surface structures with specific gene products is essential to understand the mechanisms of the pathogen life cycle. We have applied an AFM-based immunolabeling technique for the proteomic mapping of macromolecular structures through the visualization of the binding of antibodies, conjugated with nanogold particles, to specific epitopes on *Bacillus* spore surfaces. This information is generated while simultaneously acquiring the surface morphology of the pathogen. The immunospecificity of this labeling method was established through the utilization of specific polyclonal and monoclonal antibodies that target spore coat and exosporium epitopes of *Bacillus atrophaeus* and *Bacillus anthracis* spores.

INTRODUCTION

Atomic force microscopy (AFM) provides unique capabilities for imaging *in vitro* the architecture, assembly and structural dynamics of both single macromolecules and large macromolecular ensembles at near-molecular resolution. In particular, significant progress has been achieved in the last decade in AFM probing of DNA, DNA-protein complexes, [1-4] membrane proteins, [5-10] pathogens (in particular, viruses [11-17] and bacterial spores[18-25]), and macromolecular crystallization.[26-28]

AFM provides high-resolution topographical information about the spatial and temporal distribution of macromolecules in biological samples. However, it lacks chemical specificity, in particular on the identification of antigens. The identification of specific macromolecules in AFM images has been conducted based on their size and shape. For example, specific globular proteins can be identified in a heterogeneous biological sample based on molecular weight and corresponding size, as was done for the outer membrane of *Chlamedia trachomatis* bacterium.[28] Chemical force microscopy[29] was successfully utilized for the mapping of molecular interactions on the surfaces of biological entities, which provides means for specific molecular recognition.[30-33] In the past several years, considerable progress, in particular towards probing of microbial and cellular systems, has been made in identification and mapping of specific receptors and ligands on the biological surfaces using adhesion force mapping and dynamic recognition force mapping (for reviews, see [34,35]). However, simultaneous near molecular-resolution topographical imaging of biological structures and specific recognition of the proteins forming these structures is currently lacking.

Of particular importance is the identification of the protein composition of pathogen surfaces. Pathogen outer surface structures (e.g. virus membranes and capsids, as well as bacterial cell walls, spore coats and exosporia) typically contain multiple proteins. While it is known to a certain degree which proteins are expressed for these surface structures, it is often unknown which of these are exposed on the outside of these structures and which are embedded within the structures. Detection of surface-exposed proteins is paramount for improving the fundamental understanding of their functional properties as well as for the development of detection, attribution and medical countermeasures against these pathogens.

Electron microscopy (EM)-based immunolabeling techniques have become an important tool for the elucidation of biological structure and function.[36-38] These techniques provide means for identification and localization of a protein of interest using antibodies raised against it. Epitope mapping using monoclonal antibodies (mAbs) is a powerful tool for examining the surface topology of macromolecules. Through its binding specificity, each mAb defines one specific site on the antigen's surface. Colloidal gold, first introduced by Faulk and Taylor in 1971[37] is universally utilized in EM for identification, localization and distribution of proteins of interest at an ultrastructural level. However, to produce images with the highest resolution and contrast, electron microscopy techniques require sample preparation methods such as fixation, staining, dehydration, embedding and thin sectioning, that may potentially damage the epitopes or make them less accessible. In contrast, AFM-based methods are capable of probing biological systems with spatial resolution similar to EM techniques; but without requiring treatments that may alter the delicate native structure of biological specimens.

AFM immunogold markers were utilized in the past for imaging of proteins, macromolecular ensembles and protein-protein interactions. These include mapping of gold-labeled photosystem I on thylakoid membranes,[40] visualization of protein fibrinogen,[41] heparin binding sites on single fibronectin molecules,[42] and visualization of interaction of nanogold RGD-peptide and integrin receptors.[43] First demonstrations of feasibility of using immunogold markers in AFM imaging of microbial and cellular systems has been reported in studies of human lymphocytes,[44] where immunogold particles were clearly resolved from the cell surfaces. More recently AFM–based immunolabeling was utilized to demonstrate biochemical distinction between types I and II collagen fibers.[45] These immunolabeling experiments were performed on air-dried cellular samples. First *in situ* observation of immunolabeling by AFM was reported in studies of mapping of bacteriorhodopsin purple membrane with non-labeled antibodies.[46] Recently, AFM-based immunogold labeling of fully hydrated mycobacterial cells was reported.[47]

In this study, we have utilized AFM- based immunochemical labeling procedures for visualization and mapping of the binding of antibodies, conjugated with nanogold particles, to specific epitopes on the surfaces of *Bacillus anthracis* and *Bacillus atrophaeus* spores.

B. anthracis, the causative agent of anthrax, is a Gram-positive spore forming bacterium.[48, 49] For *B. anthracis* spores, the outermost structure is the exosporium, which is a loose-fitting layer that envelops the spore.[50] The exosporium is composed of a paracrystal basal layer and an external hair-like nap layer extending up to 600 nm in

length.[51] Approximately 20 exosporium-associated protein and glycoprotein species have been identified.[51-55]

The outermost structure of *B. atrophaeus* spores is the spore coat, for which approximately 50 *Bacillus* proteins or protein orthologs have been identified by genomic/proteomic analysis.[56] (*B. atrophaeus* spores have been utilized as a biological stimulant for decontamination and sterilization processes [57,58] (and bioaerosol detection development.[59,60] We have recently utilized AFM to unravel native structures of various dormant and germinating bacterial spores, including *B. atrophaeus* [21,23,24]and *C.novyi-NT* species.[25]

In this report, we describe the development of AFM for immunolabeling of the *B. anthracis* exosporium and of the *B. atrophaeus* spore coat. Control AFM experiments, which are required to validate the specificity and avidity of immunochemical labeling, were often absent in prior publications describing AFM-based immunolabeling experiments. Here, we highlight experimental procedures and control experiments which establish the validity of AFM-based immunolabeling experiments..These control experiments demonstrate that AFM can be utilized for visualization and topological mapping of antigen-antibody interactions on native spore surfaces. The immunospecificity of labeling was established through the utilization of specific polyclonal (pAbs) and monoclonal (mAbs) antibodies that target spore coat and exosporium epitopes.

MATERIALS AND METHODS

Spore preparation. *Bacillus anthracis* cultures were grown for Sterne FC26 (containing only one of the two virulence plasmids, pXO1) as well as for plasmid-less ΔSterne. The cultures were grown on Brain Heart Infusion (BHI) broth (Difco, Detroit, Michigan.) at 37°C. A platform shaker set to 150 rpm was used for agitation. Prior to the onset of sporulation, the cells were removed from the incubator, concentrated by centrifugation, and plated on nutrient agar containing 31 mg/L $MnSO_4$. The plates were incubated at 37°C and sporulation was monitored with phase-contrast microscopy. Incubation times varied between 3 and 5 days. At harvest, water-soluble media components were removed by centrifuging and washing the pellet with sterile water (x3). The pellet was subsequently re-suspended in water and stored at 4°C until analysis. *B. atrophaeus* spores were prepared and purified as described in [61]. Spore preparations were stored at 4°C.

Immunolabeling. Rabbit anti- *B. atrophaeus* 270696-01 (A B-BgN)[61] and rabit anti- *B. anthracis* 070497-02[62], monoclonal mouse anti- *B. anthracis* antibodies and 18 nm secondary gold-labeled rabbit and goat antibodies, 18 nm gold-labeled rabbit IgG and were obtained from Dr. T.J. Leighton (Children's Hospital Oakland Research Institute).

For immunolabeling experiments, spores were suspended in phosphate buffered saline (PBS, pH 7.4) containing 0.5% bovine serum albumin (BSA) for 15 min and then were incubated for 1-2 hours with the relevant concentrations of primary antibodies diluted in PBS/0.5% BSA buffer. The suspension was then centrifuged for 5 min at 14,000g, while the supernatant was discarded. The pellet was washed 3-5 times through consecutive re-suspension with PBS containing 0.5% BSA for 15 minutes, followed by

centrifugation for 5 m in at 14,000g and removal of the supernatant. After being washed in PBS/0.5% BSA, spore suspensions were incubated for 1-2 hours with appropriate concentrations of secondary gold-labeled antibodies diluted in PBS/0.5% BSA buffer. The suspension was then centrifuged for 3 m in at 14,000 g, and the supernatant was discarded. The pellet was washed through consecutive re-suspensions with PBS/0.5% BSA (3 times), twice with PBS and several times with double distilled water as described above. Antibody-labeled spores suspended in double distilled water were utilized in AFM experiments.

For gold enhancement experiments, a GoldEnhance TM-EM reagent (Nanoprobes, Yaphank, New York) consisting of four solutions was utilized. Equal amounts of Solution A (enhancer) and Solution B (activator) were incubated for 5 m in followed by the addition of equal amounts of Solution C (initiator) and Solution D (buffer). A mixture of the gold enhance solutions was incubated for 20 m in with a suspension of antibody-labeled spores suspended in water. The suspension was centrifuged for 5 m in at 14,000g and the supernatant was discarded. The pellet was washed 3 times through consecutive re-suspension with double-distilled water, followed by centrifugation for 5 m in at 14,000g and removal of the supernatant. Antibody-labeled spores suspended in double distilled water were utilized in AFM experiments.

Atomic force microscopy. After immunolabeling, droplets of ~ 2.5 µl of spore suspensions containing the antibody-labeled spores were deposited on plastic cover slips and incubated for 10 minutes, after which the sample substrate was carefully rinsed with double-distilled water and allowed to dry. Images were collected using a Nanoscope IV

atomic force microscope (Veeco Instruments, Santa Barbara, California) operated in tapping mode. For rapid low-resolution analysis of spore samples, fast scanning AFM probes (DMASP Micro-Actuated, Veeco Instruments, Santa Barbara, California) with resonance frequencies of ~ 210 kHz were utilized. The typical radius of the DMASP AFM tip radius is ~ 10 nm, which is comparable with the size of the gold nanoprobes utilized in immunolabeling experiments. Because of the convolution of the AFM probe shape with that of the nanogold particles, the lateral sizes of the particles appear enlarged in AFM images. For high-resolution imaging, SuperSharp Silicon (SSS) AFM probes (NanoWorld Inc, Neuchâtel, Switzerland) with tip radius < 2nm and resonance frequencies of ~ 300 kHz were used, for which tip convolution is much less. Tapping amplitude, phase and height images were collected simultaneously. To better show the presence of the antibody-gold complexes on the spores, the AFM height images were typically 'contrast enhanced' (standard part of the Veeco AFM software package).

AFM antibody distribution analysis. Since the actual spore labeling was done in solution before the spores where deposited on the plastic substrate, we assume that the density of antibodies over the spore surface is uniform, *i.e*. the coverage is the same for the bottom part of the spore attached to the substrate and the exposed top part. Because of the surface-imaging nature of AFM, we can only see the top half of a spore deposited on the sample substrate, *i.e*. 50% of the total spore surface. The finite sharpness of AFM tips reduces the accessible surface a bit further. While in our experiments we have utilized high-aspect-ratio AFM probes with an average aspect ratio of 4:1 and a small half cone opening angle < 10° (both defined at 200 nm from the tip apex), at the outer spore edges

the orientation of the spore surface still approaches a 90° angle with respect to the spore's central top part and hence this spore periphery cannot be imaged with the AFM tip. We estimate that this inaccessible edge area represents 10 % of the top half of the spore surface, *i.e*. 5% of the total surface spore area, which leaves 45% of the spore surface accessible to AFM. Thus, to calculate the total amount of Abs per spore from the observed amount, we have multiplied the latter by 1/0.45 = 2.22.

In addition to the amount of antibodies (Abs) per single spore, we also calculated the density of antibodies on spores (in Abs/ μm^2) to compare this number with the Abs/μm^2 density on the background (*i.e*. on the substrate). To estimate the spore surface area, we employed the formula used to calculate the surface area A of a prolate spheriod (cigar-formed) object,

$$A = 2\pi(b^2 + a^2 o\varepsilon / \tan(o\varepsilon)) \quad ; \text{with} \quad o\varepsilon = \arccos\frac{b}{a} \qquad (1)$$

where a and b are the semi-major and semi-minor axis length, respectively, to estimate the total surface area of the spore. The comparison of antibody densities on spores and background is performed to exclude the influence of possible unbound antibodies in the 2.5 µl droplet sedimenting on the substrate-attached spores and inadvertently being counted as specifically bound antibodies.

RESULTS AND DISCUSSION

The AFM-based immunolabeling method described in this report is based on the visualization of the specific binding of gold-tagged antibodies to the target epitopes on bacterial spore surfaces . For the development of these procedures, we initially used polyclonal rather than monoclonal antibodies. Polyclonal antibodies are less difficult to

produce and hence less expensive, have greater epitopic range, and are far less sensitive to alterations in the target surface than are monoclonal antibodies. The goal of these initial experiments was to develop procedures that assess the specificity and avidity of immunochemical labeling.

In our first experiments, we aimed to test the validity (immunospecificity, strength of antigen-antibody binding and avidity) of immunochemical labeling through several control experiments. In order to establish the specificity of labeling, we utilized rabbit anti-*B. atrophaeus* 270696-01 (AB-BgN) and goat anti-*B. atrophaeus* (AB-BgD) polyclonal antibodies, which were targeted to spore coat epitopes,[61] and we used non-specific rabbit IgG as a control. These primary antibodies were labeled either with secondary antibodies or Protein A (data are not shown), both tagged with 18 nm gold particles. These preliminary experiments indicated the specificity of the utilized antibodies. As illustrated in Fig. 1a,b, a number of gold-labeled anti-*B. atrophaeus* polyclonal antibodies are seen bound to the spore coat, while binding of non-specific rabbit IgG (Fig. 1c,d) is virtually absent. In other control immunolabeling experiments (Figs. 1e,f), we also utilized a gold enhancement reagent, which catalytically deposits metallic gold onto the pAb- and IgG-associated nanogold particles, drastically increasing the size of the nanogold particle. Large gold features were seen in the case of spore-bound gold-enhanced anti-*B. atrophaeus* pAbs (Fig. 1e), while in control experiments (Fig. 1f), these features were absent. In another negative control labeling experiment (data are not shown), the primary antibody was omitted and only gold-labeled antibodies was utilized, which was found not to bind to the spore coat surface. These initial control

experiments de monstrate that AFM can be ut ilized for visualization and topological mapping of specific antigen-antibody interactions on native spore surfaces.

We then exam ined the immunol abeling for the exosporium of *Bacillus anthracis Sterne* spor es with rab bit anti- *B. anthracis* polyclonal antibody 070497-02, [62] ta rgeted against exo sporium surface protein s and non-sp ecific IgG as a control. Again, both antibodies were labe led with seco ndary an tibodies tagged with 18 nm gold. In each experiment, we analyzed ~ 100 ind ividual sp ores th rough im aging of multiple ~ 4 x 4 μm^2 areas, each containing on average 4-6 spores (Fig. 2a). At this m agnification, individual Ab/gold complexe s could easily be discerne d, and hence the number of antibodies on the spores could be assessed and quantified. Im aging of single spores allows visualization of gold-labeled antibodies at higher resolution (F ig. 2b-h). Note that in Fig.2e, a dom ain struc ture is seen on the spore surface, which is indicative of a basal exosporium paracrystalline layer. [50] In this case, it seem s a s though a hair-like nap is missing, which probably resulted in a low dens ity of bound antibod ies. Occasionally, as shown in Fig. 2h, a very high number of gold-labeled anti- *B. anthracis* polyclonal antibodies is seen bound to the surface of spore exosporia.

For control experim ents, IgG that was labeled with secondary antibodies, which were in turn tagged with 18 nm gold particle s, was used. In these control experim ents, virtually no antibodies are seen bound to the spore exosporium surfac es (Fig. 3a-f). In another, specificity-related, negative control experim ent we used a *B. anthracis* spore preparation in which spores were not released from their mother cells (sporangia) during sporulation and hence their exosporia where not exposed on the outside. W ith

immulolabeling, we observed no significant affinity of anti-*B. anthracis* polyclonal antibodies to the sporangia surface (Fig. 3g).

In the immunolabeling experiment shown in Fig. 2, the amount of bound rabbit anti-*B. anthracis* polyclonal antibodies on the surface of spore exosporium varied broadly from less than 10 antibodies to more than 150, with an average number of 62. To arrive at these numbers, the observed numbers of spores were multiplied by 1/0.45, the AFM-accessible area being 45 %. With average semi-major and semi-minor spore axis $a = 0.7$ μm and $b = 0.345$ μm measured for the 76 analyzed spores (Fig. 4a), the total surface area A of *B. anthracis Sterne* spores A was estimated to be 2.6 μm^2, and its AFM-accessible area was $A_{acc} = 0.45\% A = 1.16$ μm^2. Hence, the densities of anti-*B. anthracis* polyclonal antibodies bound to the surface of spore exosporia varied from 4 to 65 pAb μm^{-2} with an average density of ~ 24 pAb μm^{-2} (Fig.4b).

As a control, we have measured the density of gold-labeled antibodies bound to the substrate surface, which was found to be much lower at only ~ 1.5 pAb μm^{-2}. Hence, we can positively identify the pAbs seen on spore surfaces (Fig.2) as spore-bound pAbs, and rule out that they were pAbs sedimented onto the spores during drying of the sample prior to AFM imaging. For the control experiments with non-specific gold-labeled IgG (Fig.3a-f), the pAb the average density of bound antibodies measured from 70 spores was found to be ~ 0.4 pAb per spore (0.1 pAb μm^{-2}), while the density of pAbs bound to the substrate was estimated to be 0.2 pAb μm^{-2}.

In immunolabeling experiments, illustrated in Fig. 3g, for 67 spores on average 2 pAb per spore (0.8 Ab μm^{-2}) were observed on the sporangia and a density of 0.4 pAb μm^{-2} was found on the substrate. Thus, the affinity of anti-*B. anthracis* polyclonal

antibodies for sporangia is ~ 30 times lower than that for exosporia.

Aging of the *B. anthracis* spore preparation appears to decrease the binding affinity of anti-*B. anthracis* polyclonal antibodies to the exosporium. Thus, we have conducted experiments where the same spore preparation and labeling protocols were utilized for immunolabeling experiments six month later than the experiments described above. In these experiments, the average number of exosporium-bound anti-*B. anthracis* pAbs measured on 80 spores (Fig.4) decreased to ~14.5 per spore (~ 5.4 pAb μm^{-2}), with a substrate density of 0.5 pAb μm^{-2}, which implies a lower affinity of 62/14.5 = 4.3 as compared with the initial experiments. In this case, IgG control experiments (performed as described above) resulted in densities of 0.3 pAb per spore (0.1 Ab μm^{-2}) and a substrated density of 0.6 pAb μm^{-2} (Fig.4b).

Following completion of the above proof-of-principle AFM immunolabeling experiments targeting the *Bacillus* spore coat and exosporium with polyclonal antibodies, we proceeded with monoclonal antibody studies to investigate the proteomic composition and patterning of the *B. anthracis* spore surface. For this, we utilized mAbs specific to the *B. anthracis* exosporium glycoprotein BclA. Immunogold-electron microscopy studies recently demonstrated that BclA is the major component of the hair-like filaments present on the outer layer of the *B. anthracis* exosporium.[54]

In these AFM monoclobal antibody immunolabeling experiments, the number of anti-BclA gold-labeled mAbs bound to the surface of the spore exosporium (Fig.5 a-e) was measured for 100 individual spores (Fig.6). It was found to be on average 25 mAb per spore (10 mAb μm^{-2}), with variance in the range of 2 mAb per spore (~ 0.8 mAb μm^{-2}) to 82 mAb per spore (~ 32 mAb μm^{-2}) The density of gold-labeled mAbs on the

substrate was 1.1 mAb μm^{-2}. In three sets of control experiments with 1) IgG labeled with secondary gold-tagged antibodies (Fig.5,f-j), 2) gold-tagged secondary antibodies only (Fig.7a,b), and 3) labeling with mAbs and secondary gold-tagged Abs of spores still encased in sporangia (as described above for experiments with pAbs), 0,0 and 2.8 mAb μm^{-2} bound antibodies were found on the surfaces of ~ 70, 60 and 35 spores respectively. The density of antibodies on the substrate surface was found to be ~ 0.5, 0.4 and 0.8 Ab μm^{-2} respectively. Interestingly, in the experiments with spores encased in sporangia, we occasionally observed spores that were partially removed from the sporangium sacculus (Fig. 7 c,d). The exposed spore surfaces exhibited a considerable amount of gold-labeled mAbs indicating the presence of BclA protein, once more indicating the specificity of the applied immunolabeling method.

In this study, we have established the validity (strength of antigen-antibody binding and avidity) of immunochemical labeling of the exosporium of *Bacillus anthracis* and the spore coat of *Bacillus atrophaeus* spores through various control experiments. We have further established the immunospecificity of labeling, through the utilization of specific anti-*B. atrophaeus and B. anthracis* polyclonal and monoclonal antibodies, which were targeted to spore coat and exosporium epitopes. The AFM immunolabeling experiments presented here have confirmed that bclA glycoprotein is the immuno-dominant epitope on the surface of *B. anthracis* spores.

These experiments demonstrate that AFM can be utilized for visualization and topological mapping of antigen-antibody specific interactions on surfaces of bacterial spores. Bacterial spores exist in the environment in the dehydrated state. Thus, the development of capabilities for AFM probing the protein composition on air-dried spore

surfaces is relevant and important for their detection, attribution and forensic reconstruction of the production and processing methods of spore preparations. Note, that in the experiments presented here, we have visualized antibodies conjugated with 18 nm colloid gold particles. Smaller colloidal gold particles or 1-2 nm probes of gold atoms based on ordered gold chelates may also be utilized, as long as they can be morphologically discerned from other (pathogen) structures.

More generally, the further development of *in vitro* AFM immunolabeling technique for probing of architecture, assembly and structural dynamics of biological systems under physiological conditions is of significant importance. . The ability to directly visualize antigen-antibody complexes on the native surfaces of single pathogens has broad-ranging implications for the fundamental understanding of the pathogens' life cycle and development of medical countermeasures,. For example, we have recently utilized AFM to probe *in vitro* the structural dynamics of single germinating spores with high resolution. [24] The combination of these experiments with AFM-based immunolabeling techniques could allow the identification of spore coat proteins that play a role in spore germination, and provide a structural understanding of how these proteins regulate spore survival, germination and disease.

The feasibility of *in vitro* AFM-based immunolabeling of biological systems was recently demonstrated. [47] However, significant improvements in the methodology, including a broad range of control and validation experiments and further enhancement of resolution are required.

ACKNOWLEDGEMENTS

This work was performed under the auspices of the U.S. Department of Energy by the Lawrence Livermore National Laboratory under Contract DE-AC52-07NA27344. This work is supported by the Lawrence Livermore National Laboratory through Laboratory Directed Research and Development Grant 04-ERD-002. We would like to acknowledge Terrance Leighton, Katherine Wheeler and Olivia Mooren for providing us with antibodies and assistance in the development of immunolabeling protocols, and Sue Martin for providing us with *B. anthracis* spore preparations.

FIGURE LEGENDS

Figure 1. AFM images of specific and non-specific binding of polyclonal antibodies to the *B. atrophaeus* spore coat. (a,b) Binding of gold-labeled anti- *B. atrophaeus* polyclonal antibody to the spore coat. Numerous gold-labeled antibodies are seen bounded to the spore surface. In (a), the area imaged enlarged in (b) is indicated with a white box. (c,d) A corresponding control experiment with non-specific gold-labeled IgG. In (c), the area imaged enlarged in (b) is indicated with a white box. (e,f) Utilization of gold enhancers for growth of nanogold particles in case of anti- *B. atrophaeus* polyclonal gold-labeled antibody bound to the spore coat (e) and non-specific gold-labeled IgG (f). Images presented in Fig.1 were acquired with fast-scanning AFM probes. All other AFM images presented in this article were acquired using super sharp AFM probes.

Figure 2. AFM images of specific binding of anti-*B. anthracis* polyclonal antibodies to the *B. anthracis* spore exosporia. (a) A group of six spores with gold-labeled polyclonal antibodies bounded to spore surfaces. (b-g) Higher-resolution images of the individual spores of the group visualized in (a). (h) A spore with a very high pAb density.

Figure 3. AFM images of non-specific binding of IgG labeled with secondary antibodies to the *B. anthracis* spore exosporia. (a) A group of 5 spores. (b-f) Higher-resolution images of the individual spores of the group imaged in (a). In (a-f), virtually no bound gold-labeled antibodies are seen on spore surfaces. (g) AFM image of non-specific binding of anti- *B. anthracis* polyclonal antibodies to spores encased in sporangia show the absence of bounded gold-labeled antibodies.

Figure 4. Statistics of pAbs bound on *B. anthracis* spores (a) Distribution plot of bound pAbs on B. *anthracis* spores. Initial experiment with fresh spore suspension (black bars) and with the same, 6-month old spore suspension (white bars). The number of bound pAbs is observed to decrease, with a lower spread, on the older spore preparation. (b) Average pAb density per *B. anthracis* spore (left axis) or number of pAbs per spore (right axis) for various experiments (see text): I: Initial pAb experiment. II:.Initial IgG control. III: pAb experiment performed 6 months later. IV: IgG control 6 months later. V: pAbs on sporangia. VI: IgG on sporangia control. For (I-VI): Dark grey (left): density on spores; left grey (right): density on background (control, left axis only).

Figure 5. AFM images of specific (a-e) and (the absence of) non-specific (f-j) binding of anti-BclA gold-labeled monoclonal antibodies to *B. anthracis* spores. Higher-resolution images of the group imaged in (f) are presented in (g-j).

Figure 6. Statistics of mAbs bound on *B. anthracis* spores (a) Distribution plot of bound mAbs on *B. anthracis* spores. (b) Average mAb density per *B. anthracis* spore (left axis) or number of mAbs per spore (right axis) for various experiments (see text): I: mAb experiment; II:. IgG control. III: mAbs on sporangia. IV: secondary antibody control. For (I-IV): Dark grey (left): density on spores; left grey (right): density on background (control, left axis only).

Figure 7. AFM images of control experiments. (a) Image showing the absence of spore

surface bou nd gold-lab eled second ary antibod ies. (b -d) In general, anti-BclA g old-labeled m onoclonal antibodies do n ot bind to th e surface o f sporangia. In this case, the spores' exosporia su rfaces are no t expose d., (c, d) Bound mAbs are seen only on spore surfaces, which are ob served to b e partiall y rem oved from the spora ngium sacculus, indicating the high specificity of the mAbs for the exosporia.

TOC Figure legend

AFM im ages of specific binding of anti- *B. anthracis* polyclonal antibodies to the *B. anthracis* spore exosporia.

REFERENCES

1. Hoh, J. H.; Lal, R.; John, S.A.; Re vel,J.P.; Arnsdorf, M.F. *Science 253*, **1991**, 1405-1408.
2. Hansma, H.G. *Ann. Rev. Phys. Chem.* **2001**, *52*, 71-92.
3. Lyubchenko, Y.L.; Shlyakhtenko, L.S.; Aki, T.; Adhya, S. *Nucleic Acids Res.* **1997**, *25*, 873-876.
4. Lyubchenko, Y.L. *Cell Biochem. and Biophys*. **2004**, *41*, 75-98.
5. Schabert, F. A.; Henn, C.; Engel, A. *Science* **1995**, *268*, 92-94.
6. Müller, D.J.; Fotiadis, D.; Engel, A. *FEBS Lett*. **1998**, *430*, 105-111.
7. Engel, A.; Müller, D.J. *Nature Struct. Biol*. **2000**, *7*, 715-718.
8. Fotiadis D.; Liang, Y.; Filip ek, D.A.; Saperstei n, D.A.; Engel, A.; Palczewski, P. *Nature* **2003**, *421*, 127-128.
9. Bahatyrova, S.; Frese, F .N.; Siebert, C.A.; Olsen, K.O.; van der W erf, K.O.; van Grondelle, R.; Niederman, R.A.; Bullough, P.A.; Otto, C.; Hunter, C.N. *Nature* **2004**, *430*, 1058-1062.
10. Frese, R.N.; Siebert, C.A.; Nieder man, R.A.; Hunter, C.N.; Otto, C.; van Grondelle, R. *Proc. Natl. Acad. Sci. USA* **2004**, *101*, 17994-17999.
11. Kuznetsov, Yu.G.; Malkin, A.J.; Lucas, R.W.; Plomp, M.; McPherson, A. *J. Gen. Virol.* **2001**, *82*: 2025-2034.
12. Kuznetsov, Yu.G.; Datta, S.; Kothari, N.H.; Greenwood, A.; Fan, H.; McPherson, A. *Biophys. J.* **2002**, *83*, 3665-3674.
13. Kuznetsov, Yu.G.; Victoria, J.G. ; Robinson, Jr.W .E.; McPherson. A. *J. Virol.* **2003**, *77*, 11896-11909.

14. Malkin, A. J.; McPherson, A.; Gershon**,** P.D. *J. Virol.* **2003**, *77*, 6332-6340.

15. Kiselyova, O.I .; Yam insky, I.V.; Karpova, O.V.; Rodionova, N.P.; Kozlovsky, S.V.; M.V. Arkhipenko, M.V.; Atabekov, J.G. *J. Mol. Biol*. **2003**, *332*, 321-325.

16. Malkin, A.J.; M. P lomp, M.; McPherson, A. In *DNA viruses. Methods and Protocols*; P.M. Liberman, Ed.; Humana Press: Totowa, 2005; pp. 85-108.

17. Malkin, A.J.; Kuznetsov, Yu.G.; Plomp, M.; McPherson, A. In *Structure-based study of viral replication*; Cheng, R.H., Miayamura,T. Eds.; World Scientific Pub. Co: Singapore, 2008, pp. 289-310.

18. Dufrêne, Y.F.; Boonaert, C.J.P.; G erin, P.A.; Asther, M.; Rouxhet, P.G. *J Bacteriol*. **1999**, *181*, 5350-5354.

19. Chada, V.G.R., Sanstad, E.A.; W ang, R.; Driks, A. *J Bacteriol.* **2003**, *185*, 6255-6261.

20. Dufrêne Y.F. *Nature Reviews. Microbiol.* **2004**, *2*, 451-458.

21. Plomp, M., Leighton, T.J.; W heeler, K.E.; Malkin, A.J. *Biophys. J.* **2005**, *88*, 603-608.

22. Plomp, M., Leighton, T.J.; W heeler, K.E.; Malkin, A.J. *Langmuir* **2005**, *21*, 7892-7898.

23. Plomp, M., Leighton, T.J.; W heeler, K.E.; Pitesky, M.E.; Malkin, A.J. *Langmuir* **2005,** *21*, 10710-10716.

24. Plom p, M., Leighto n, T.J.; W heeler, K.E.; Hill, H.D.; Malkin, A.J. *Proc. Nac. Acad. Sci.* **2007**, *104*, 9644-9649.

25. Plom p, M.; McCaffery, J.M.; Cheong, I.; Huang, X.; Bettegowda, C.; Kinzler, K.W.; Zhou, S.; Vogelstein, B.; Malkin**,** A.J. *J. Bacteriol*.**2007,** 189, 6457-6468.

26. Malkin, A.J.; Kuznetsov, Yu.G.; Land, T.A.; DeYoreo, J.J.; McPherson, A. *Nature Struct Biol.* **1995**, *2***,** 956-959.

27. Yau, S.T.; Thomas, B.R.; Vekilov, P.G. *Phys. Rev. Lett.* **2001**, *85 (2)*, 353-356.

28. Malkin, A. J.; McP herson, A. In *From solid-liquid interface to nanostructure engineering*; Lin, X.Y.; DeYoreo, J.J., Eds.; Plenum/Kluwer Academic Publisher: New York, 2004; Vol. 2, pp. 201-238.

29. Noy, A. *Surf. And Interface Anal.* **2006**, *38*, 1429-1441.

30. Florin, E.L.; Moy, V.T.; Gaub, H.T. *Science* **1994**, *264*, 415-417.

31. Hinterdorfer, P.; Baum gartner, W .; Gruber, H.J.; Schilcher, K.; Schinder, H. *Proc. Natl. Acad. Sci. USA* **1996**, *93*, 3477-3481.

32. Stroh,C.; W ang, H.; Bach, R.; Ashcroft , B.; Nelson, J.; Gruber, H.; Lohr, D.; Lindsay, S.M.; Hinterdorfer, P. *Proc. Natl. Acad. Sci. USA* **2004**, *101*, 12503-12507.

33. Hinterdorfer, P.; Dufrêne, Y.V. *Nature Methods* **2006**, *3*, 347-355.

34. Dufrêne, Y.F., Hinterdorfer, P. *Eur. J. Physiol.* **2008**, 256, 237-245.

35. Dufrêne, Y.F. *Nature Microbiology Reviews* **2008**, 6, 674-680

36. Stirling, J.W. *J. Histochem. And Cytochem.* **1990**, *38*, 145-157.

37. Robinson, J.M.; Takizawa, T.; Vandre, D. *J. Microscopy* **2000**, *199*, 163-179.

38. Bendayan, M. *Science* **2001**, *291*, 1363-1365.

39. Faulk, W.P.; Taylor, G.M. Immunochem. **1971**, *8*, 1081-1083.

40. Kaftan, D.; Brumfeld, V.; Nevo, R.; Scherz, A.; Reichen, Z.; *EMBO J*., **2002**, 21, 6146-6153.

41. Soman, P.; Rice,Z.; Siedlecki, C.A. *Micron*, **2008**, *39*, 832-842.

42. Lin,H.; Lal,R.; Clegg, D.O. *Biochemistry*, **2000**, *39*, 3192-3196.

43. Hussain, M.A.; Agnihotri, A.; Siedleci, C.A.; *Langmuir* **2005**, *21*, 6979-6986.

44. Putman, C.A.J.; de Grooth, B.G.,; Hansma, P.K.; van Hulst, N.F. *Ultra microscopy* **1993**, *48*, 177-182.

45. Arntz, Y.; Jourdainne, L.; Greiner-W acker, G.; Rinckenbach, S.; Ogier, J.; Voegel, J.-C.; Lavalle, P.; Vautier, D. *Microscopy Research and Technique* **2006**, *69*, 283-290.

46. Müller, D.J.; Schoenenberger, C.-A.; Büldt, G.; Engel, A. *Biophysical J*. **1996**, *70*, 1796-1802.

47. Alsteens, D. ; Verbelen, C.; Dague, E.; Raze, D.; Baulard, A.R.; Dufrene, Y.F. *Eur. J. Physiol.* **2008**, *456*, 117-125.

48. Cote, C. K.; Chabot, D.J.; Scorpio, A.; Blank, T.E.; Day, W .A.; Welkos, S.L.; Bozue, J.A. In *Microorganisms and bioterrorism*. M. B endinelli, M., Ed.; Springer, New York 2006, pp. 83-111.

49. Mock, M.; Fouet, A. *Annu. Rev. Microbiol.* **2001**, *55,* 647-671.

50**.** Gerhardt, P.; Ribi, E. *J. Bacteriol.* **1964**, *88*, 1774-1789.

51. Redm ond, C., Baillie, L.W .J; Hi bbs, S.; Moir, A.J.G; Moir, A. *Microbiology* **2004**, *150*, 355-363.

52. Steichen, C.; Chen, P.; Kearney, J.F.; Turnbough, Jr., C.L. *J. Bacteriol*. **2003**, *185*, 1903-1910.

53. Steichen, C. T.; Kearney, J.F.; Turnbough, Jr., C.L. *J. Bacteriol*. **2005**, *187*, 5868-5876.

54. Sylvestre, P.; E. Couture-Tosi, E.; Mock, M. *Mol. Microbiol.* **2002**, *45*,169-178.

55. Sylvestre, P., E.; Couture-Tosi, E.; Mock, M. *J. Bacteriol*. **2005**, *187*, 5122-5128.

56. Kim H.; Hahn, M.; Grabowski, P.; Mc Pherson, D.C.; Otte, M.M.; W ang, R.; Ferguson, C.C.; Eichenberger, P.; Driks, A. *Mol Microbiol*. **2006**, *59*, 487-502.

57. Fritze, D.; Pukall, R. *Intl. J. of System. And Evolut. Microbiol.* **2001**, *51***,** 35-37.

58. Penna T.C.V.; Marques, M.; Machoshvili, I.A. *Appl. Biochem. And Biotech.* **2002**, *98***,** 539-551.

59. Burke, S. A.; W right, J.G.; R obinson, M.K.; Bronk, B.V.; W arren, R.L.; *Appl. and Environm. Microbiol*. **2004**, *70*, 2786-2790.

60. Fergenson D.P.; Pitesky, M.E.; Tobias, H.J.; Steele, P .T.; Czerwieniec, G.A.; Russell S.C.; Lebrilla, C.B.; Horn, J.M.; Coffee, K.R.; Srivastava, A.; Pillai, S.P.; Shih, M.T.P.; Hall, H.L .; Ram poni, A.J.; Chang, J.T.; Langlois, R.G.; Estacio P.L.; Hadley, R.T.; Frank, M.; Gard, E.E. *Anal.Chem*. **2004**, 76, 373-378.

61. Longchamp P.; Leighton, T. *Lett. App. Microbiol.***2000***, 31*,242-246.

62. Longchamp P.; T. Leighton. T. *J. App. Microbiol.* **1999**, *87*, 246-249.

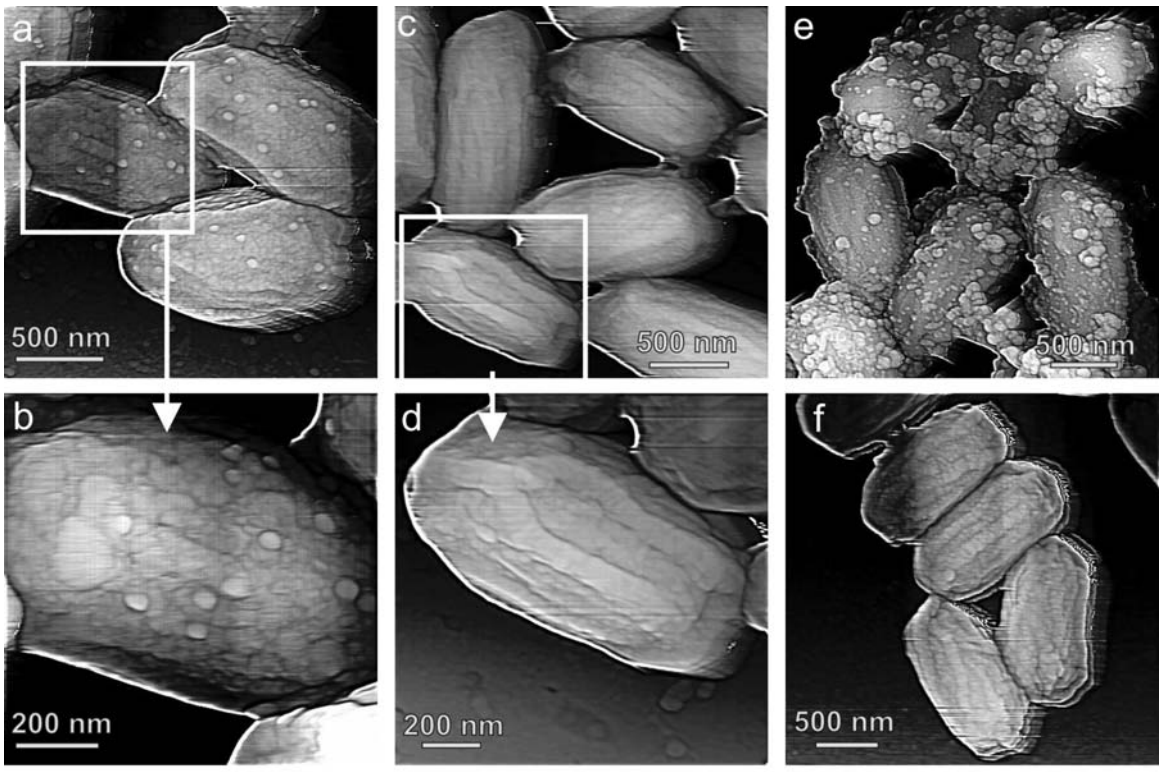

Figure 1

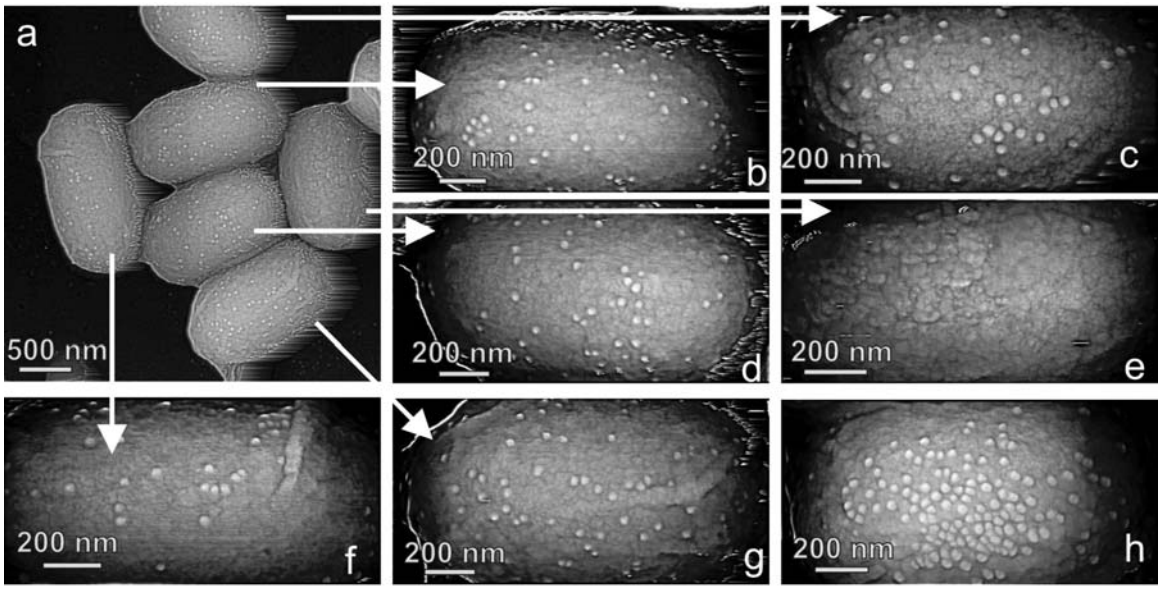

Figure 2

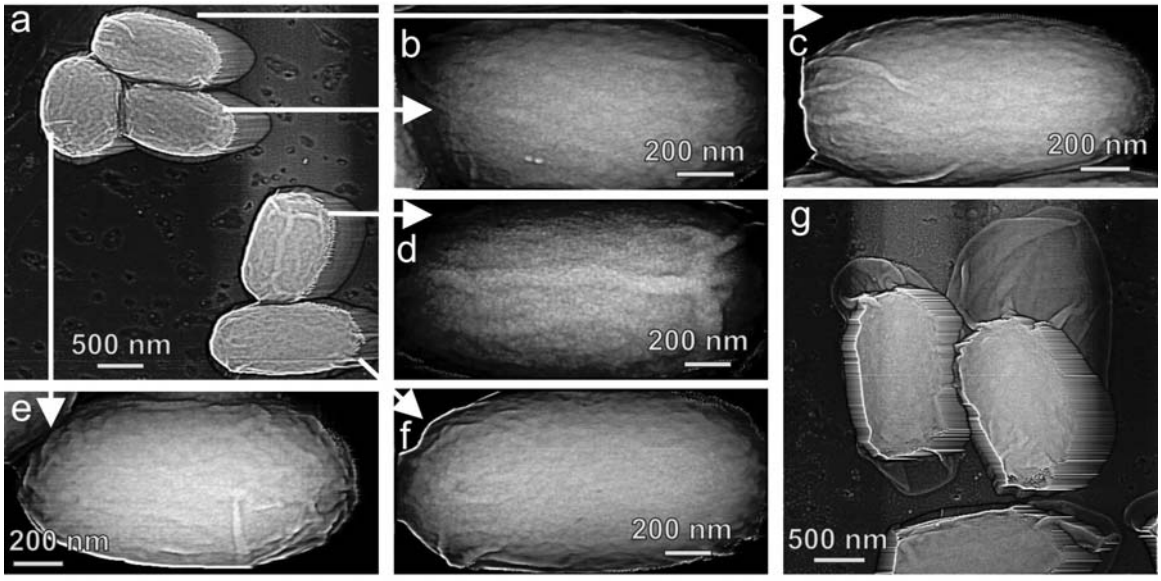

Figure 3

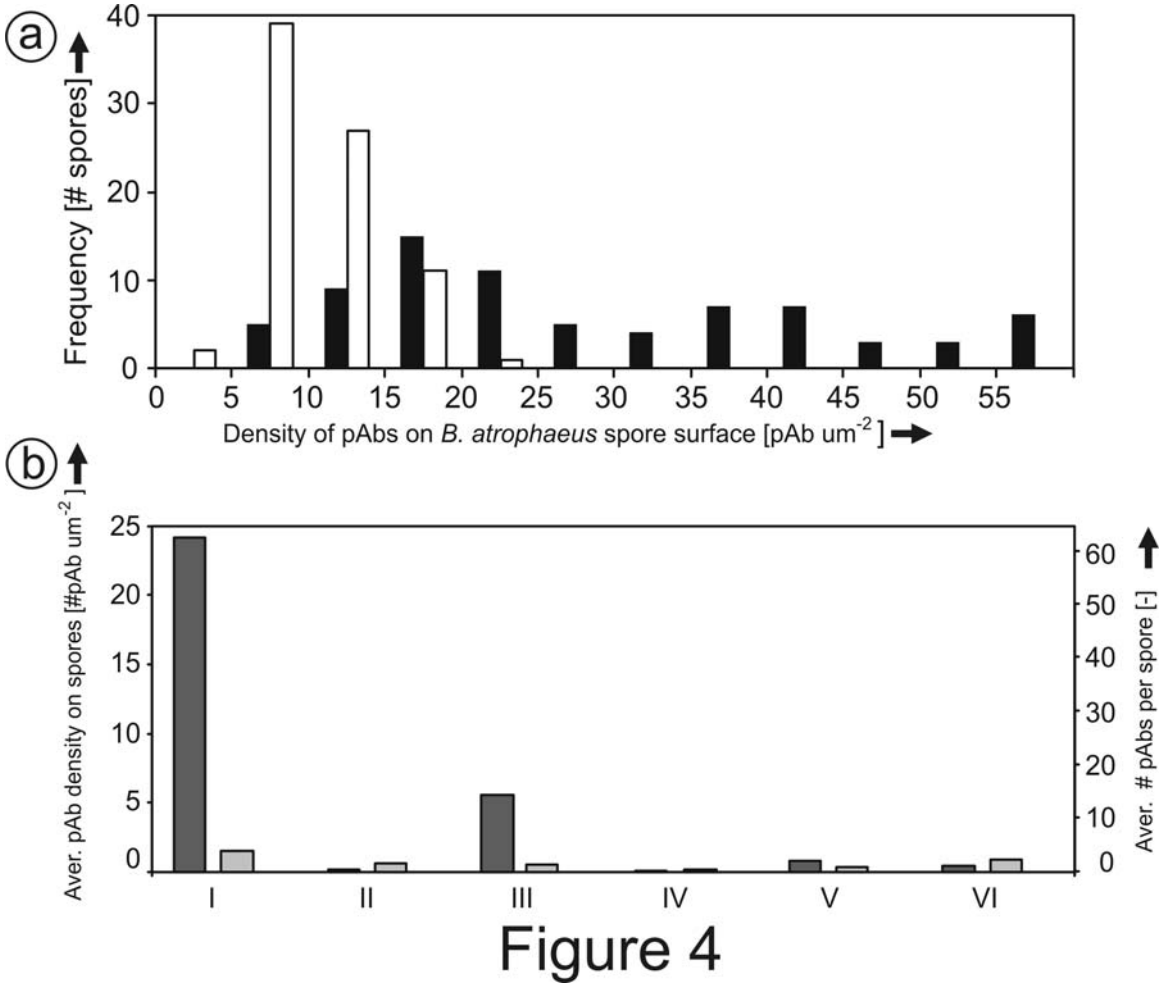
a
Frequency [# spores]
0
10
20
30
40
0
5
10
15
20
25
30
35
40
45
50
55
Density of pAbs on B. atrophaeus spore surface [pAb um-2]
b
Aver. pAb density on spores [#pAb um-2]
0
5
10
15
20
25
Aver. # pAbs per spore [-]
0
10
20
30
40
50
60
I
II
III
IV
V
VI

Figure 4

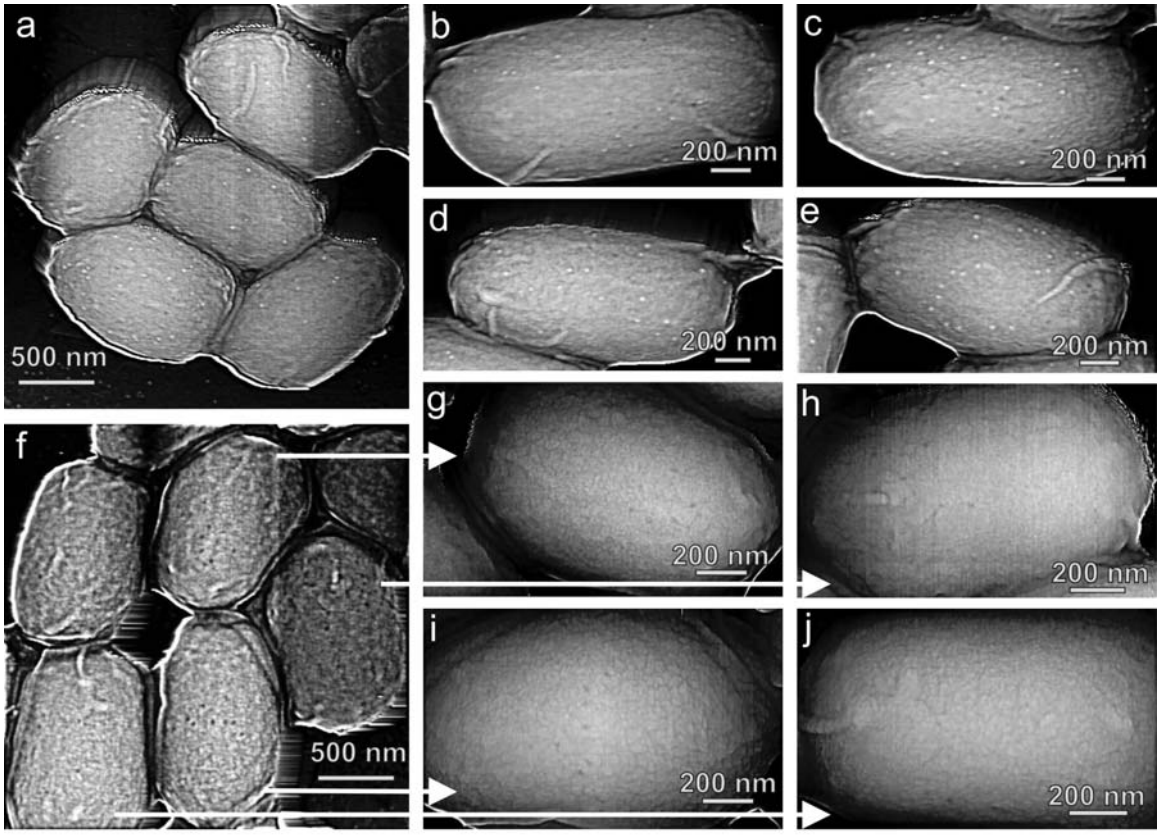
a
500 nm
b
200 nm
c
200 nm
d
200 nm
e
200 nm
f
500 nm
g
200 nm
h
200 nm
i
200 nm
j
200 nm

Figure 5

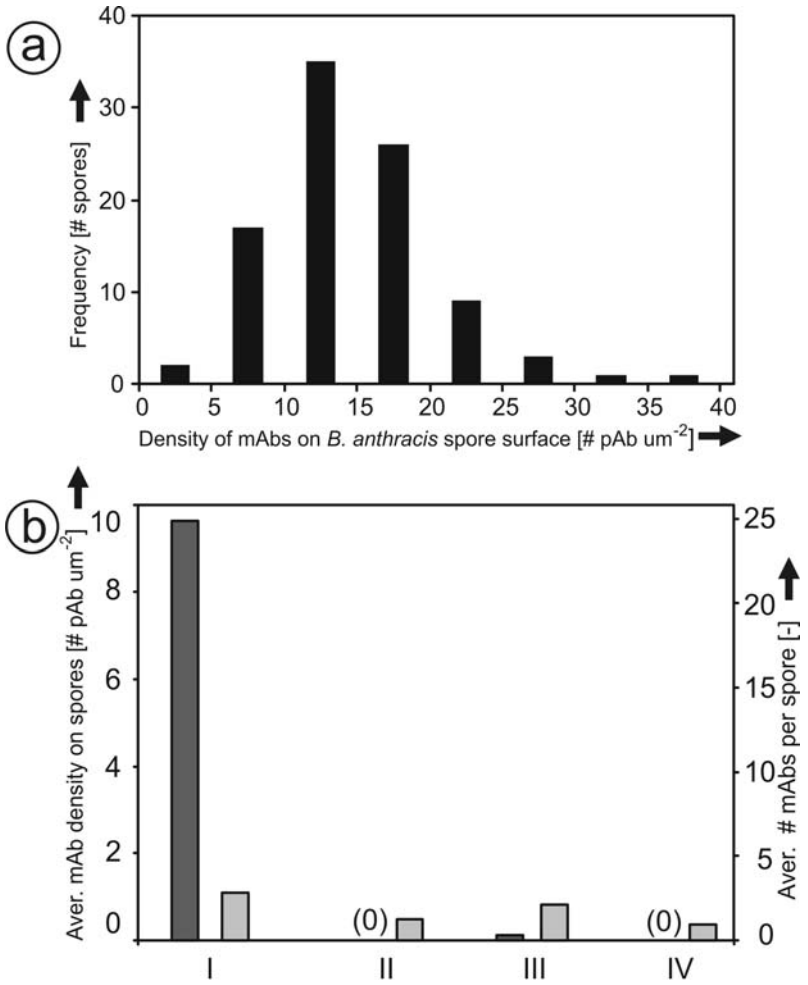
a
Frequency [# spores]
Density of mAbs on B. anthracis spore surface [# pAb um-2]
b
Aver. mAb density on spores [# pAb um-2]
Aver. # mAbs per spore [-]
(0)
(0)
I
II
III
IV

Figure 6

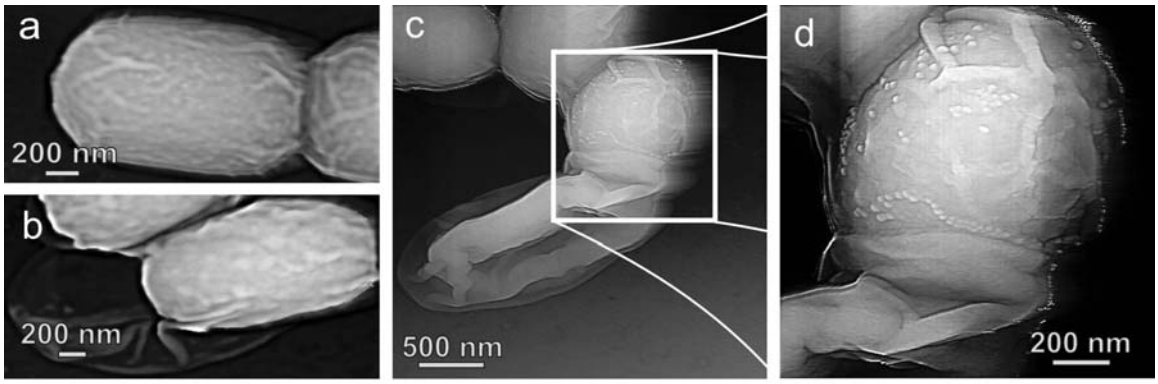

Figure 7

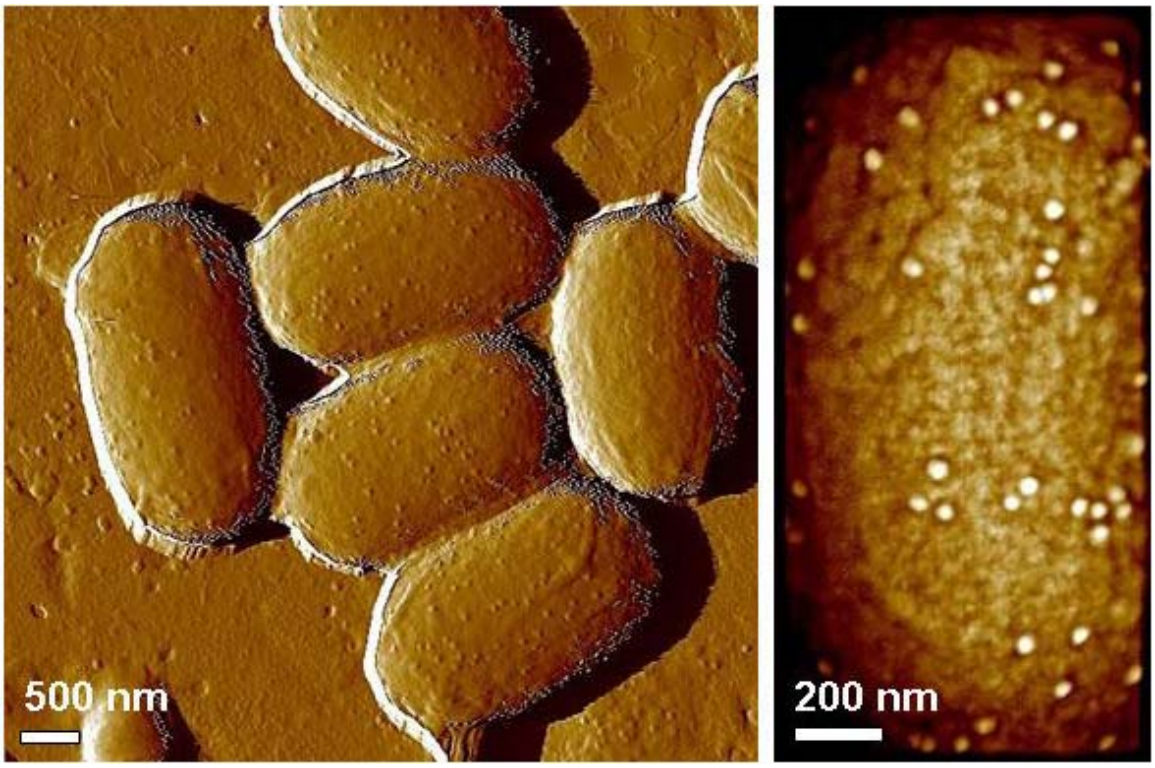

Table of Contents Graphic